Local burning behavior of wind-driven flames under the influence of mixed-convective turbulent flow conditions

Alankrit Srivastava and Ajay V. Singh
Indian Institute of Technology, Kanpur
Kanpur - 208016, Uttar Pradesh, India

1 Introduction

Most naturally occurring fires involve turbulence interactions that can affect the combustion kinetics and heat feedback mechanism in boundary layer diffusion flames [1-2]. Also, the turbulent fire spread generally occurs in a mixed-convective environment where large density gradients give rise to the strong buoyant forces which uplift the flame from the fuel surface. In contrast, the crossflow momentum pushes the flame toward the fuel surface [3]. Furthermore, the mass burning rate is an essential fundamental factor affecting the flame spread rate over a given condensed fuel surface. The average mass burning rate measurements are readily available, but the problem lies in estimating the local mass burning rate, which helps understand the physics of boundary layer combustion.

Earlier, Singh et al. [4] developed a theoretical relation to determine the local mass burning rate for boundary layer diffusion flames stabilized over a condensed fuel surface. Following the work of Emmons et al. [5] and using Reynolds analogy, the authors developed a unique mass burning rate correlation, as indicated in Eqn. (1). Here, B is the Spalding mass transfer number, k_w is gas-phase thermal conductivity calculated at wall temperature, c_p is the specific heat of air calculated at the adiabatic flame temperature, Pr is the Prandtl number, L is the length of the pyrolysis zone, $(\partial T^*/\partial y^*)_{y^*=0}$ is the non-dimensional temperature gradient evaluated at the fuel surface, and $y^* = y/L$ represents the non-dimensional distance in the crossflow direction. In addition, T^* represents the non-dimensionalized temperature defined as $(T - T_{w,p})/(T_{fl,ad} - T_{w,p})$, where $T_{w,p}$ is the wall temperature in the pyrolysis zone, and $T_{fl,ad}$ is the adiabatic flame temperature of the given fuel. Various experiments were performed to validate this model for laminar boundary layer diffusion flames stabilized over a liquid and solid fuel surface [4,6]. More recently, Singh et al. [2] tested the given theoretical model (Eqn. (1)) for turbulent boundary layer diffusion flames using lightly-sooting ethanol fuel. The authors found that the given correlation works well under turbulent flow conditions. However, the authors suggested that more testing on heavily-sooting fuel is needed to remark on the general validity of the proposed correlation.

$$\dot{m}_f^{''} = \frac{Bk_w}{c_p L}(Pr)^{2/3}\left(\frac{\partial T^*}{\partial y^*}\right)_{y^*=0} \quad (1)$$

In the present work, a non-dimensional parameter was defined to observe the competitive impact of buoyancy, momentum, and turbulence on boundary layer flames occurring in a mixed-convective

Correspondence to: ajayvs@iitk.ac.in

regime. The proposed correlation considers the property of a given fuel, resulting in a generalized form that can help in predicting the local mass burning rates of condensed fuel surfaces. The current study utilized the experimental data of a sooty fuel (n-heptane) and a lightly-sooting fuel (ethanol) to examine the burning characteristics of turbulent wind-driven flames stabilized under different flow conditions. A unified mass burning rate correlation was developed in the present work to understand the local burning characteristics of turbulent boundary layer diffusion flames.

2 Experimental facility and data analysis

Fig. 1 illustrates the schematic of the test apparatus used for studying wind-driven flames under turbulent flow conditions. A laboratory-scale wind tunnel was used for generating variable crossflow conditions. The fuel wick ($25\ cm \times 8\ cm \times 1.27\ cm$) was prepared according to the procedure suggested by Singh et al. [6] to limit the burning to the top surface. In addition, for reducing flow separation and bluff body effects, a thin metallic sheet ($40.64\ cm \times 7\ cm \times 0.1\ cm$) was placed before the fuel wick. The entire assembly was placed over a high-precision load cell that monitored the overall mass loss of the fuel sample for the specified period. R-type fine-wire thermocouples of wire diameter 50 μm were used for temperature measurements at high spatial resolution using a traverse mechanism. A data acquisition card (NI 9214) was used to acquire, condition, and digitalize the voltage signals from the thermocouples, where the measurement was conducted at a sampling rate of 100 samples/second for 10 sec at the specific location. Due to the usage of fine-wire thermocouples, the conduction errors were negligible (<1%) for this study. Also, while accommodating the radiation correction based on the approach given by Singh et al. [6], the error in local temperature gradients was found to be considerably lower. Hence, thermocouple radiation error was not considered in this study.

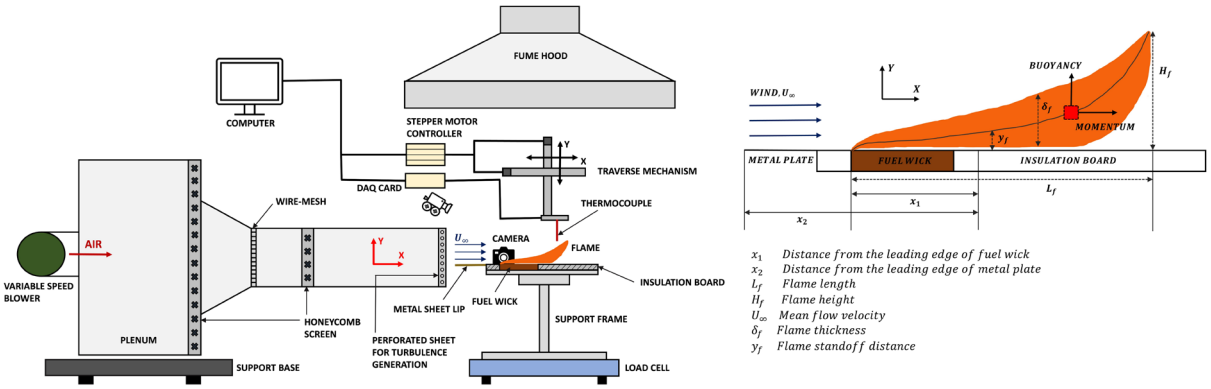

Fig. 1. Schematic of the experimental setup and the structure of boundary layer diffusion flame.

Grid-based freestream turbulence was introduced in the flow path based on the work of Zhou et al. [1]. Various grids or wire mesh (Table 1) were installed at the exit section of the wind tunnel to obtain the desired turbulence intensity. Flow characterization was performed with the help of a constant temperature hot-wire anemometer (CTA), where the data for average flow velocity and turbulence intensity was recorded at the leading edge of the fuel surface. While maintaining the dwell time of 60 seconds, the measurements were recorded (50,000 samples/sec) by traversing the hot-wire anemometer normal to the fuel surface. The turbulence intensity (TI) can be expressed as $TI = u'/U_\infty$, where u' and U_∞ is defined as the root mean square (RMS) of velocity fluctuations and average flow velocity, respectively. The current study considered the crossflow velocity and turbulent intensity variation from 1 m/s to 1.8 m/s and 3% to 9%, respectively. Also, a Nikon D7000 digital camera was used to record side videos of the flame which were further processed in an image processing algorithm developed in MATLAB, as performed by Singh et al. [2]. Each experiment was repeated at least five times, and the overall uncertainty associated with velocity, load cell data, temperature, and flame parameter measurements, was found to be less than 3%, 2%, 4%, and 2.5%, respectively.

Table 1. Turbulence grid details

Grid	Hole/Wire diameter	Center-to-center distance	Blockage ratio (BR)	Formula to evaluate blockage ratio
Grid 1	1.6 mm	3.2 mm	0.77	$1-\frac{(\text{ hole diameter })^{2*}0.9089}{(\text{center-to-center distance })^2}$
Grid 2	3 mm	d_H = 6 mm d_V = 7 mm	0.83	$1-\frac{(\text{ hole diameter })^{2*}0.785}{(d_H)*(d_V)}$
Wire Mesh	1.5 mm	14.7 mm	0.18	$1-\frac{(\text{center-to-center distance})^2*1}{(\text{center-to-center distance }+\text{ wire diameter })^2}$

d_H – Horizontal distance, d_V – Vertical distance

3 Results and discussions

3.1 Flame characteristics

Table 2 shows the flame parameter values corresponding to various freestream conditions for n-heptane flame. It can be seen that there is a significant increase in the flame length with an increase in crossflow velocity. In contrast, the flame length showed a decreasing trend with increasing turbulence intensity for the same flow velocity. This flame shortening can result from quenching or combustion enhancement due to turbulence. Furthermore, a decreasing trend was observed for the flame height with increased crossflow velocity, which followed hydrodynamic and thermal boundary layer theory [7]. However, no definite trend in flame height was noticed with respect to turbulence intensity. Furthermore, the flame standoff distance (distance measured from the fuel surface to the center of the flame zone) is an essential parameter as it governs the amount of heat received by the virgin fuel surface. Fig. 2 (a) depicts the non-dimensional variation of flame standoff distance along the downstream direction for different crossflow conditions. It can be observed that the flame standoff distance showed an increasing trend for a given crossflow condition in the streamwise direction. Also, at a given *x*-location and with the same turbulence intensity, the flame standoff distance decreases upon increasing the freestream velocity. This drop can be linked to the hydrodynamic and thermal boundary layer theory, where the flow with a higher Reynolds number decreases the boundary layer thickness [7]. In addition, for the particular flow velocity, flame standoff distance showed a decreasing trend with increasing turbulence intensity due to enhanced mixed combustion.

Table 2. The flame parameter values for various crossflow conditions.

Flame property	**U_∞ = 1 m/s TI = 5%**	**U_∞ = 1 m/s TI = 9%**	**U_∞ = 1.8 m/s TI = 3%**	**U_∞ = 1.8 m/s TI = 9%**
Flame Length (cm)	28.25	27.05	37.84	34.33
Flame Height (cm)	7.66	9.45	4.75	3.86

The momentum and buoyancy have a competitive effect that governs the burning dynamics of wind-driven flames. Following the early works of Zhou et al. [1], a local forced-flow variable (ψ_{x_2}) was defined to account for both momentum and turbulence, as presented in Eqn. (2). Here, u'/U_∞ represent the turbulent intensity and v_f is the kinematic viscosity of air at mean film temperature. The mean film temperature (T_f) is calculated as $T_f = (T_{fl,ad} + T_w)/2$, where $T_{fl,ad}, T_w$ represents the fuel adiabatic flame temperature and wall surface temperature, respectively. Here, 'a' is the constant dependent on the fuel properties and orientation of the fuel surface.

$$\psi_{x_2} = \mathrm{Re}_{x_2}^{1/2}\left(1 + a(u'/U_\infty)^{1/2}\right) = \left(\frac{U_\infty x_2}{v_f}\right)^{1/2}\left(1 + a(u'/U_\infty)^{1/2}\right) \quad (2)$$

More recently, Singh et al. [2] also used a similar flow variable that considered the value of a = 0.47 for ethanol fuel, obtaining the best empirical fit that yields some important correlations. However, there is

a need for a generalized correlation that would work for any particular fuel using some fuel property. Thus, to incorporate the chemical characteristic of the fuel, the constant 'a' was expressed as a function of mass transfer number (B), as presented in Eqn. (3). Also, a local Grashof number (Gr_{x_1}) was introduced to account for buoyancy effects, as represented by Eqn. (4). Here, β_f is the coefficient of thermal expansion calculated at the mean film temperature $\left(\beta_f = 1/T_f\right)$ and g is the acceleration due to gravity. Further, the combined influence of buoyancy, momentum, and turbulence can be represented in the form of a non-dimensional variable (ξ_x) as given in Eqn. (5). The proposed correlation can be used for any given fuel under both laminar as well as turbulent crossflow conditions. The exponent 'n' values utilized in most studies are 3, 4, and 5, and similar values were also employed in this investigation. To characterize the local burning behavior of wind-driven flames, the best empirical fit was obtained for the calculated value of a = 0.577 for n-heptane and a = 0.458 for ethanol [7], along with a value of n = 3. In this regard, non-dimensional standoff distance was plotted against ξ_x (Fig. 2 (b)) and a fitting relation was obtained for both fuels as represented in Eqn. (6).

$$a = \frac{\ln(1+B)}{2.6\,B^{0.15}} \tag{3}$$

$$\mathrm{Gr}_{x_1} = \frac{g\beta_f(T_{fl,ad}-T_w)x_1^3}{v_f^2} \tag{4}$$

$$\xi_x = Gr_{x_1}/\psi_{x_2}^n \tag{5}$$

$$y_f^* = 0.0856(\xi_x)^{0.18} \tag{6}$$

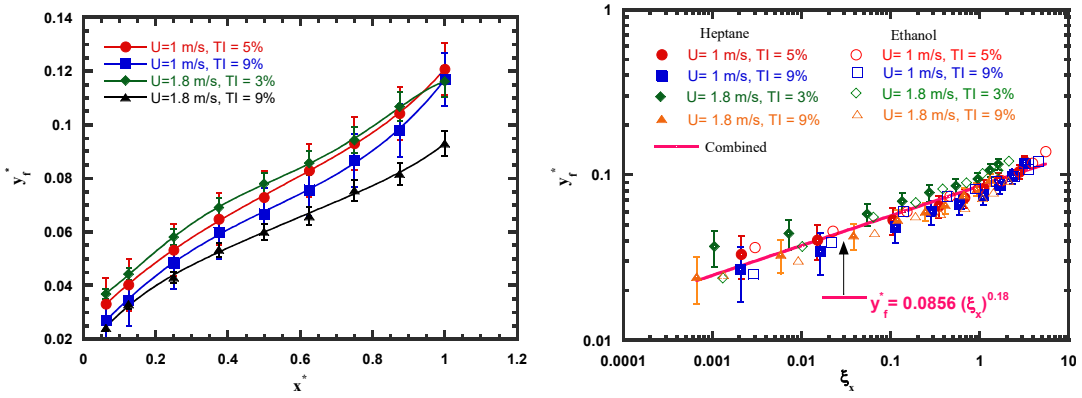

Fig. 2. Non-dimensional flame standoff distance variation (a) along streamwise direction. (b) with respect to ξ_x. The non-dimensional scale was based on the length of the fuel wick (80 mm).

3.2. Local mass burning rate

The local mass burning rate was evaluated using the theoretical correlation presented in Eqn. (1). Table 3 summarizes the validation of the theoretical correlation, where the mean mass burning rate (measured using a load cell) is compared against the averaged local mass burning rates measured at various streamwise locations, which showed a maximum error of 19%. This concludes that the correlation based on the Reynolds analogy (Eqn. 1) applies to turbulent boundary-layer flames as well. Further, to examine the relationship with other flame parameters, the local mass burning rate was non-dimensionalized by dividing it with the product of mass transfer number (B) and corresponding characteristic buoyant mass flux ($\dot{m}_b''$), as represented in Eqn. (7). The non-dimensional local mass burning rate was plotted against the non-dimensional flame standoff distance $\left(y_f^*\right)$, as shown in Fig. 3 (a). It was observed that the local mass burning rate decreases with increasing flame standoff distance, as reported in earlier studies [2,6]. In this regard, an inverse relation was obtained, as presented in Eqn. (8). Also, to characterize the mass burning rate in a mixed-convective regime, the non-dimensional local mass burning rate $\left(m_f^*\right)$ was plotted against ξ_x for both heptane and ethanol flames, as shown in Fig. 3 (b). A power-law fit was

observed between the two variables, as presented in Eqn. (9). Eqn. (9) represents a unified correlation between the non-dimensional local mass burning rate (m_f^*) and ξ_x for a specific fuel (defined by B number). This correlation can be further rewritten in another form, as presented in Eqn. (10). In addition, both local and average mass burning rates can be predicted using the correlation presented in Eqns. (9) and (10) for wind-driven flames occurring under laminar and turbulent crossflow conditions. The main benefit of using the new local mass burning rate relation (Eqn. (10)) over the relationship presented in Eqn. (1) is that it simply utilizes the knowledge of surface temperature and adiabatic flame temperature of a given fuel instead of detailed temperature profiles close to the fuel surface to evaluate non-dimensional temperature gradients at the fuel surface. A validation study for this new local mass burning rate correlation is shown in Table 4, where averaged mass burning rates for both laminar and turbulent boundary-layer flames are presented. It can be observed from Table 4 that the semi-empirical correlation developed in Eqn. (10) gives a maximum error of 18.8 %. Thus, once the flow and thermal parameters are known for a specific fuel, the mass burning rate correlation presented in Eqn. (10) can be used to predict the average and local mass burning rates in turbulent boundary-layer flames.

$$m_f^* = \dot{m}_f''/B\,\dot{m}_b'' = \dot{m}_f''/B\rho_\infty\sqrt{Agx_1} \tag{7}$$

$$m_f^* = 0.00011\left(y_f^*\right)^{-1.7} \tag{8}$$

$$m_f^* = 0.00686(\xi_x)^{-0.326} \tag{9}$$

$$\dot{m}_f'' = 0.00686\,(\xi_x)^{-0.326}\,\rho_\infty\sqrt{Agx_1}\cdot B \tag{10}$$

Table 3. Verification of local mass burning rate model presented in Eqn. (1) for both fuels

Flow Conditions	Load Cell (g/m^2s)	Theoretical Correlation (Eqn. (1)) (g/m^2s)	Error (%)
n-Heptane			
U_∞ = *1 m/s, TI = 5%*	27.87	31.33	12.41
U_∞ = *1 m/s, TI = 9%*	28.57	31.86	11.52
U_∞ = *1.8 m/s, TI = 3%*	32.93	32.19	-2.25
U_∞ = *1.8 m/s, TI = 9%*	37.86	40.09	5.89
Ethanol			
U_∞ = *1 m/s, TI = 5%*	14.20	14.94	5.25
U_∞ = *1 m/s, TI = 9%*	14.26	14.66	2.80
U_∞ = *1.8 m/s, TI = 3%*	15.26	16.65	9.14
U_∞ = *1.8 m/s, TI = 9%*	15.98	19.05	19.21

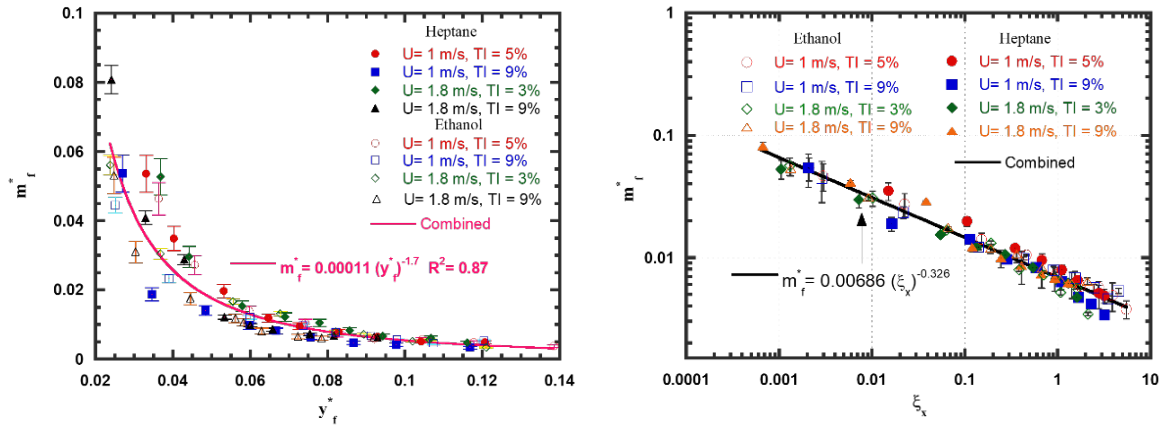

(a) (b)

Fig. 3. Variation of non-dimensional local mass burning rate with (a) non-dimensional flame standoff distance (y_f^*). (b) mixed-convective parameter (ξ_x).

Table 4 Validation of the proposed correlation (Eqn. (10)) to estimate the local mass burning rate

Flow Conditions	Load Cell (g/m^2s)	Correlation (Eqn. 10) (g/m^2s)	Error (%)
n-Heptane (Turbulent)			
U_∞ = *1 m/s, TI = 5%*	27.87	31.02	11.3
U_∞ = *1 m/s, TI = 9%*	28.57	31.38	9.83
U_∞ = *1.8 m/s, TI = 3%*	32.93	38.46	16.79
U_∞ = *1.8 m/s, TI = 9%*	37.86	42.87	13.23
Ethanol (Turbulent)			
U_∞ = *1 m/s, TI = 5%*	14.20	13.56	-4.53
U_∞ = *1 m/s, TI = 9%*	14.26	13.97	-2.03
U_∞ = *1.8 m/s, TI = 3%*	15.26	18.14	18.87
U_∞ = *1.8 m/s, TI = 9%*	15.98	18.30	14.51
Ethanol (Laminar) [6]			
U_∞ = *0.79 m/s*	12.49	10.56	-15.45
U_∞ = *0.99 m/s*	12.93	11.79	-8.81
U_∞ = *1.54 m/s*	14.12	13.74	-2.69
U_∞ = *2.06 m/s*	15.50	15.84	2.19

4 Conclusions

A systematic experimental investigation was carried out to study the burning behavior of turbulent wind-driven fires in a mixed-convective environment. The gas-phase temperature profiles near the fuel surface were used to evaluate the local mass burning rates in turbulent wind-driven flames. It was observed that the burning rate correlation based on the Reynolds analogy can be used to estimate both the local and global mass burning rates in both laminar and turbulent wind-driven fires. Moreover, a unified mixed-convection parameter $\left(\xi_x = Gr_{x_1}/\psi_{x_2}^n\right)$ was introduced to capture the effects of momentum, buoyancy, and flow turbulence in wind-driven fires, where Gr_{x_1} is the Grashof number and ψ_{x_2} is a turbulent forced-flow variable. Corresponding to the value of $n = 3$ and the fuel-specific value of 'a', a power-law fit was observed between the local mass burning rate and ξ_x, which was later used to define a unified semi-empirical mass burning rate correlation.

References

[1] L. Zhou, Concurrent Turbulent Flame Spread, Symposium (International) on Combustion. 23 (1991) 1709–1714.

[2] A. Singh, A. V. Singh, Burning behavior of mixed-convection wind-driven flames under varying freestream conditions, Fire Saf J. 122 (2021) 103320.

[3] C.H. Miller, W. Tang, E. Sluder, M.A. Finney, S.S. McAllister, J.M. Forthofer, M.J. Gollner, Boundary layer instabilities in mixed convection and diffusion flames with an unheated starting length, Int J Heat Mass Transf. 118 (2018) 1243–1256.

[4] A. V. Singh, M.J. Gollner, Estimation of local mass burning rates for steady laminar boundary layer diffusion flames, Proceedings of the Combustion Institute. 35 (2015) 2527–2534.

[5] H.W. Emmons, The Film Combustion of Liquid Fuel, Journal of Applied Mathematics and Mechanics. 36 (1956) 60–71.

[6] A.V. Singh, A Fundamental Study of Boundary Layer Diffusion Flames, Ph.D. Thesis, University of Maryland, MD, USA, 2015.

[7] J.G. Quintiere, Fundamentals of Fire Phenomena, 2006.